ELSEVIER

Ceramics International 31 (2005) 611–619

CERAMICS INTERNATIONAL

www.elsevier.com/locate/ceramint

Microstructures of partially stabilized zirconia manufactured via hybrid plasma spray process

Guy Antou[a,*], Ghislain Montavon[b], Françoise Hlawka[a], Alain Cornet[a], Christian Coddet[b]

[a] *LISS, Institut National des Sciences Appliquées de Strasbourg, 24 Bd de la Victoire, 67084 Strasbourg Cedex, France*
[b] *LERMPS, Université de Technologie de Belfort-Montbéliard, site de Sévenans, 90010 Belfort Cedex, France*

Received 26 July 2004; received in revised form 4 August 2004; accepted 28 August 2004
Available online 9 December 2004

Abstract

Air plasma spraying and in situ laser irradiation by diode laser processes were combined to modify structural characteristics of TBCs. Results show that in situ laser remelting induces: (i) the growth of a columnar dendritic structure, which is promising concerning the thermo-mechanical properties of the coating; (ii) no phase transition: the main phase still remains the metastable tetragonal (t′) phase after laser treatment; (iii) an increase of the porosity level due to the formation of large cracks (as shown by image analysis).
© 2004 Elsevier Ltd and Techna Group S.r.l. All rights reserved.

Keywords: B. Microstructure-final; D. ZrO_2; E. Thermal applications; Thermal barrier coating

1. Introduction

Yttria–partially stabilized zirconia (Y-PSZ) thermal barrier coatings (TBCs) have numerous applications as insulation layers onto gas turbine components. The working temperatures of aircraft engines reach generally 1200 °C and even higher temperatures [1]. The benefit of these coatings results from their ability to sustain high temperature gradients in the presence of adequate backside cooling. Therefore, the main function of TBCs is to enhance the engine efficiency by increasing their working temperature. Moreover, lowering the temperature of the metal substrate enhances the life of the components submitted to degradation at high temperatures, to erosion resulting from the impact of solid particles, to corrosive attacks, to oxidation, etc. [1–4]. These coatings are commonly manufactured using atmospheric plasma spray (APS) process.

Consequently, an improvement of TBC properties is searched out; i.e., higher life-time, lower thermal conductivity, higher thermal stability and improved oxidation/corrosion protection. The characteristics of TBCs strongly depends on their pore-crack architecture. Engineering the coating architecture by an adapted process is a prerequisite to modify TBC characteristics. In this study, laser remelting was combined to thermal spraying in order to modify the TBC structure: the in situ laser remelting process was implemented. The purpose was to adapt TBC characteristics during their manufacturing process, without adding one or even more additional steps.

The structural evolution of TBCs manufactured by in situ laser remelting (i.e., laser remelting using a diode laser simultaneously to atmospheric plasma spraying) is studied here and compared to the structure of as-sprayed coatings.

2. Experimental procedure

2.1. Coating manufacturing and processing parameters

Metco[1] 204NS-B yttria–partially stabilized zirconia (Y-PSZ, ZrO_2–7 Y_2O_3) was chosen as feedstock material. The experimental device was constituted by the association of a F4 dc plasma spray gun of 40 kW from Sulzer-Metco

* Corresponding author. Tel.: +33 3 88 14 47 26; fax: +33 3 88 14 47 99.
E-mail address: g.antou@caramail.com (G. Antou).

[1] Sulzer-Metco, Rigackerstrasse 16, 5160 Wohlen, Switzerland.

0272-8842/$30.00 © 2004 Elsevier Ltd and Techna Group S.r.l. All rights reserved.
doi:10.1016/j.ceramint.2004.08.001

Table 1
Selected processing parameters[a]

Parameter	Value
Nozzle diameter (mm)	6
Arc current intensity (A)	630
Argon flow rate (SLPM)	44
Hydrogen flow rate (SLPM)	13
Hydrogen ratio (%)	30
Feedstock injector diameter (mm)	1.8
Feedstock injector tip locationfrom gun centerline axis (mm)	6
Feedstock carrier gas flow rate (argon) (SLPM)	3.4
Feedstock mass rate[b] (g min^{-1})	15–25
Spray distance (mm)	120
Spray velocity (m min^{-1})	30–60
Scanning velocity (mm min^{-1})	0.3–0.6

[a] For a Sultzer-Metco F4 dc plasma torch.
[b] Feedstock mass rate was adjusted according to the spray velocity to keep constant the average deposited thickness per pass. The spray velocity was adjusted to vary the laser energy density. The scanning velocity was adjusted according to the laser energy density to keep constant the laser treated area per spray pass.

(see footnote 1) and a laser diode (3 kW, average power), exhibiting a 848 nm wavelength, from Laserline.[2] The powder was processed implementing "reference" processing parameters listed in Table 1. The feedstock mass rate was adjusted consequently with the spray velocity, itself depending on the selected laser irradiance, in order to ensure a constant deposited thickness per pass. The coatings were remelted layer by layer, as they were manufactured. The input energy effects were studied varying the spray velocity (i.e., from 35 to 60 m min^{-1}), and consequently the irradiation duration (i.e., from 1.8 to 3.1 ms, respectively). The selected processing parameters have been extensively displayed in [5]. All manufactured coatings were about 200 μm thick.

2.2. Coating structure observation

The samples were cut using a diamond saw in an oil medium, mounted in rings and infiltrated with epoxy (i.e., impregnation technique). They were then polished following standard metallographic techniques (i.e., pre-polishing and diamond slurry polishing) on an automatic polisher. Samples were observed using SEM and optical microscopy.

Moreover, samples were cooled down in liquid nitrogen and fragily fractured in order to observe the failure facieses via SEM.

2.3. Phase identification using XRD

2.3.1. Qualitative analysis

Phase composition of as-sprayed and laser treated coatings was investigated implementing a X-ray diffractometer (Siemens D500, Munich, Germany) (40 kV, 30 mA, Co $K\alpha_1$ radiation at 0.17890 nm). A 2θ scanning step of 0.02° and a measuring time between each step of 6.0 s was used to determinate the peak positions of the different ZrO_2–Y_2O_3 phases in the range of $20° < 2\theta < 110°$. The region of the (0 0 4) and (4 0 0) T′ metastable phase peaks, between 86 and 90°, was especially investigated with a scanning step of 0.01° and a measuring time between each step of 60 s [6,7].

2.3.2. Quantitative analysis

The volume fraction, V_m of the monoclinic phase was calculated according to the Toraya et al. [8] method, where V_m is:

$$V_m = \frac{PX_m}{1 + (P-1)X_m} \quad (1)$$

where the value of P was calculated by Toraya et al. [8], for the present composition, as 1.3 and for the monoclinic–tetragonal system X_m is the integrated peak intensity ratio defined by:

$$X_m = \frac{I_m(1\,1\,1) + I_m(1\,1\,\bar{1})}{I_m(1\,1\,1) + I_m(1\,1\,\bar{1}) + I_{t'}(1\,1\,1)} \quad (2)$$

where I is the integrated peak intensity from the monoclinic (m) and tetragonal (t′) phases.

Besides, it is possible to validate, for a mole fraction ratio M_c and $M_{t'}$, the relationship proposed by Miller et al. [9]:

$$\frac{M_c}{M_{t'}} = 0.88\,\frac{I_c(4\,0\,0)}{I_{t'}(4\,0\,0) + I_{t'}(0\,0\,4)} \quad (3)$$

This relationship is computed thanks to the structural factors calculated from the ionic positions given by Teufer [10] in the case of tetragonal zirconia. This analysis assumes that the diffracted intensities by the t′ and c phases are constant even when the yttria content changes.

Finally, the calculation of the yttria content is the way to determine if the coating tetragonal phase results from equilibrium or metastable tetragonal phases [6]. The calculation of yttria content within the cubic and tetragonal phases was based on the changes of lattice parameters, as described by Scott [11]:

$$a_t\,(\text{Å}) = 5.080 + 0.00349X \quad (4)$$

$$c_t\,(\text{Å}) = 5.195 - 0.00309X \quad (5)$$

where X is the $YO_{1.5}$ content in mol%.

The a_t and c_t measurements can be altered by errors in the sample positioning. The c_t/a_t ratio permits, however, to avoid these errors and only considers the goniometer accuracy.

2.4. Pore-crack network characterization

Image analysis was carried out to quantify the pore network. SEM images were discretized and analyzed using Image 1.62 software from NIH.[3] Pores and cracks were isolated from the structures implementing several filtering

[2] Laserline, Maria Trost 23, 56070 Koblenz, Germany.

[3] NIH *Image* is a public domain image processing and analysis program. It was developed at the Research Services Branch (RSB) of the National Institute of Mental Health (NIMH), part of the National Institutes of Health (NIH). NIMH, 6001 Executive Boulevard, Rm. 8184, MSC 9663, Bethesda, MD 20892-9663, USA.

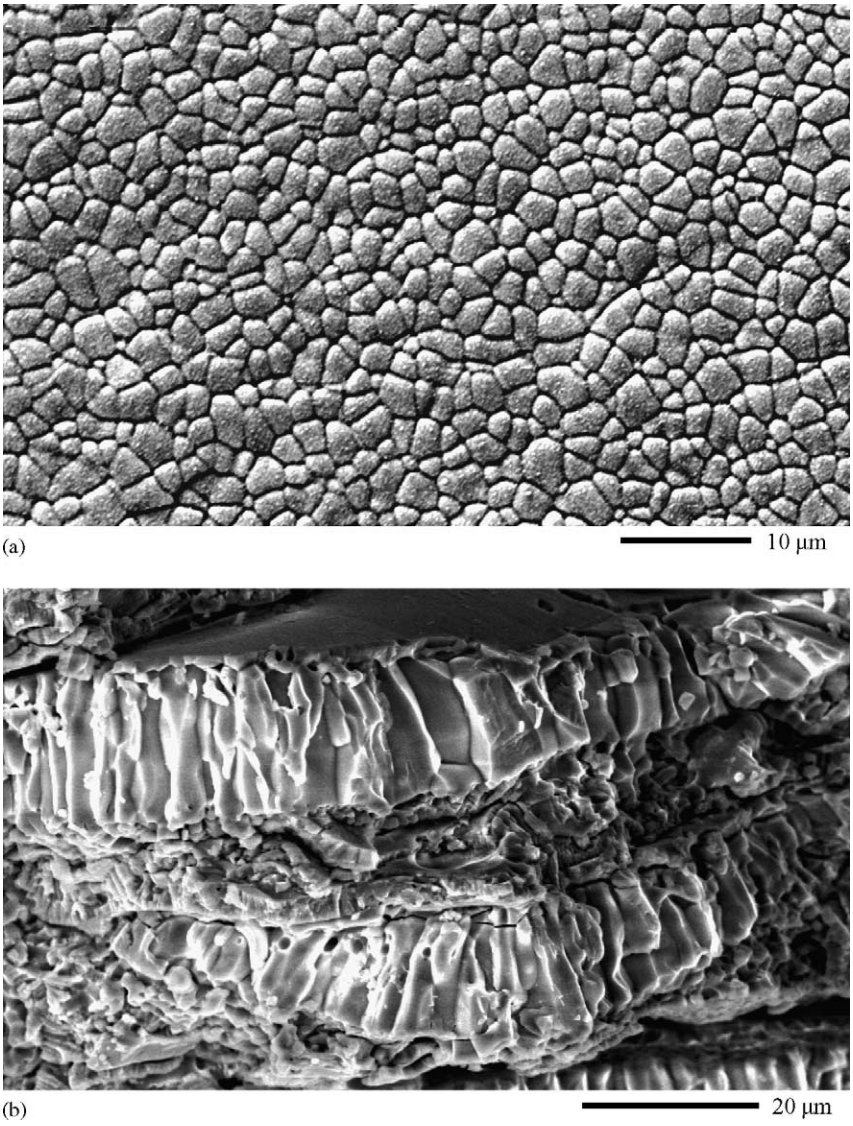

Fig. 1. Columnar dendritic structure of in situ laser remelted coating: (a) upper surface morphology and (b) fractography.

morphological protocols. Pores and cracks were then analyzed in terms of their number and their relative surface.

The cumulated length of cracks per unit surface, L_A, was calculated for each step of laser energy density in order to deduce the cumulated surface of cracks per unit volume, S_V, thanks to the following stereological relationship [12]:

$$S_V = \frac{4}{\pi} L_A \quad (6)$$

For each sample (i.e., each processing condition), the results were averaged from 15 fields of view randomly selected across the polished cross-sections.

3. Results and analysis

3.1. Microstructure

The resulting microstructure is a columnar dendritic structure (Fig. 1). Concerning in situ laser remelting, the characteristic dimension of the columnar grains is about 0.4 μm, average diameter. The microstructure orientation is typical of the directed solidification and results from the positive thermal gradient across the melt fronts generated during laser processing [13].

3.2. Subdivision of the columns

In fact, the starting point (i.e., the "base") of these columns has a characteristic dimension of 4–10 μm. Each of these starting columns divides then in smaller columns of 0.4 μm, average diameter, near the surface of the remelted layer, Fig. 2. This phenomenon is explained by the fact that the solid/liquid interfacial energy, σ, decreases near the surface. So, the free enthalpy of formation of a nucleus, ΔG_c, falls and the formation rate of nucleus, I, raises, after Eqs. (7) and (8) [14].

$$\Delta G_c = \frac{16\pi(\rho_L T_m)^2 \sigma^3 f(\beta)}{3\Delta H_m^2 \Delta T} \quad (7)$$

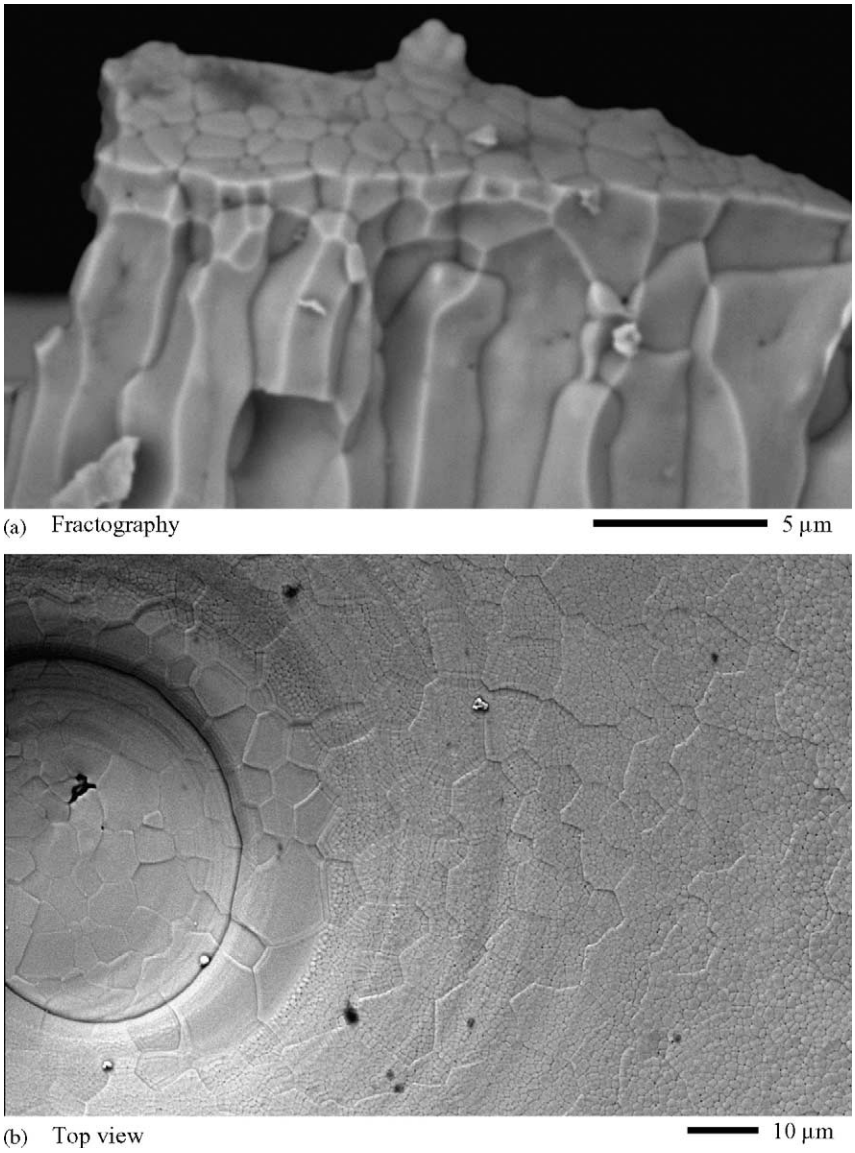

Fig. 2. (a) Fracture and (b and c) upper surface observation of remelted coating by SEM.

$$I = n_a \kappa_e \, e^{-\Delta G_c / kT} \quad (8)$$

where I is formation rate of nucleus (s^{-1}); N_a is atoms quantity into the liquid (−); κ_e is coefficient (according to the temperature) ($m\,s^{-1}\,K^{-1}$); k is Boltzmann constant ($1.38062 \times 10^{-23}\,J\,K^{-1}$); ΔG_c is free enthalpy of formation of a nucleus ($J\,kg^{-1}$); ρ_L is liquid density ($kg\,m^{-3}$); T_m is melting temperature (K); ΔH_m is solidification enthalpy ($J\,kg^{-1}$); ΔT is undercooling (K); σ is solid/liquid interfacial energy ($J\,m^{-2}$); $f(\beta)$ is effect of the surface characteristic on the nucleation.

3.3. Localized molten zones

With some laser parameters, the coating is not anymore homogeneously treated. The molten zones appear preferentially near the singularities of the surface, and are typified by the formation of craters (Fig. 3). The crater formation seems to be related to:

- gas pockets, which make their way towards the surface, thanks to the liquefaction, and suddenly release in the atmosphere. This phenomenon has been reported by some authors [15,16]. They explain that the as-sprayed ceramic top coat contains inter-splat porosity and as the ceramic melts, these pores coalesce and rise to the surface. Surface porosity is then formed when the ceramic resolidifies, before the pore has completely reached the surface;
- an open pore, which behaves like a thermal pool. In this case, the molten area expends by thermal conduction;
- an impurity within the deposit having a lower melting temperature or a higher absorption coefficient than Y-PSZ.

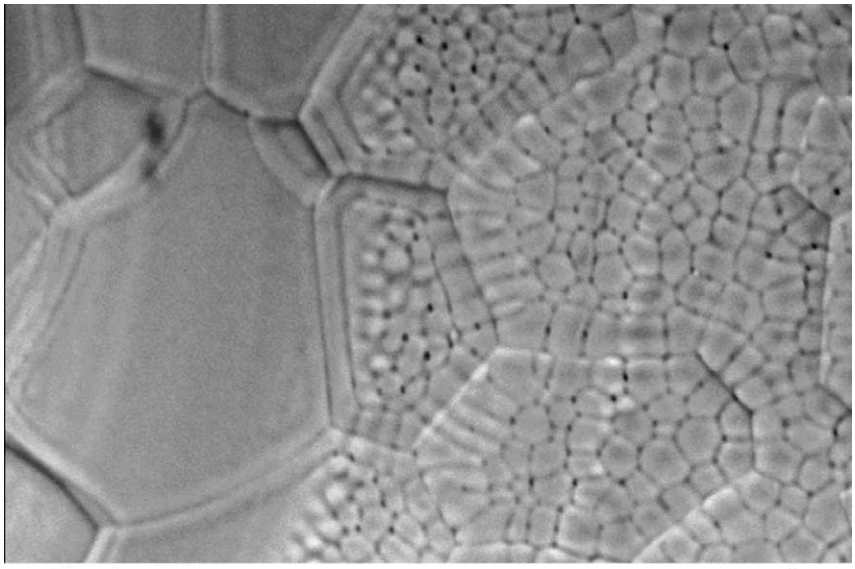

Fig. 2. (*Continued*).

3.4. Phase composition

XRD analyses with a step scanning program were carried out on the powder and on each type of manufactured coatings in two regions (for Co $K\alpha_1$ radiation): (i) from 30 to 40°, to discern the monoclinic phase from the cubic and tetragonal phases; (ii) from 86 to 90°, to differentiate the c, t and t′ phases using the separation between the $\{4\,0\,0\}_c$, the $\{4\,0\,0\}_{t,\,t'}$ and the $\{0\,0\,4\}_{t,\,t'}$ peaks. Fig. 4 presents the diffractogrammes concerning the powder, the as-sprayed and in situ remelted coatings. Table 2 lists the phase compositions of the different specimens.

3.4.1. Powder and as-sprayed coating

XRD analyses reveal that the as-sprayed coating is characterized by the predominance of the metastable tetragonal t′ phase of Y-PSZ. Moreover, there is no monoclinic phase into the as-sprayed coating, contrary to the starting powder which contains 12 mol%. The formation of this metastable t′ phase is consistent with results of previous studies [6,17–19], which have shown that, in the case of plasma spraying, the rapid solidification (i.e., $\sim 10^6$ K s^{-1}) consecutive to the impact of the molten particles leads to the formation of the t′ phase.

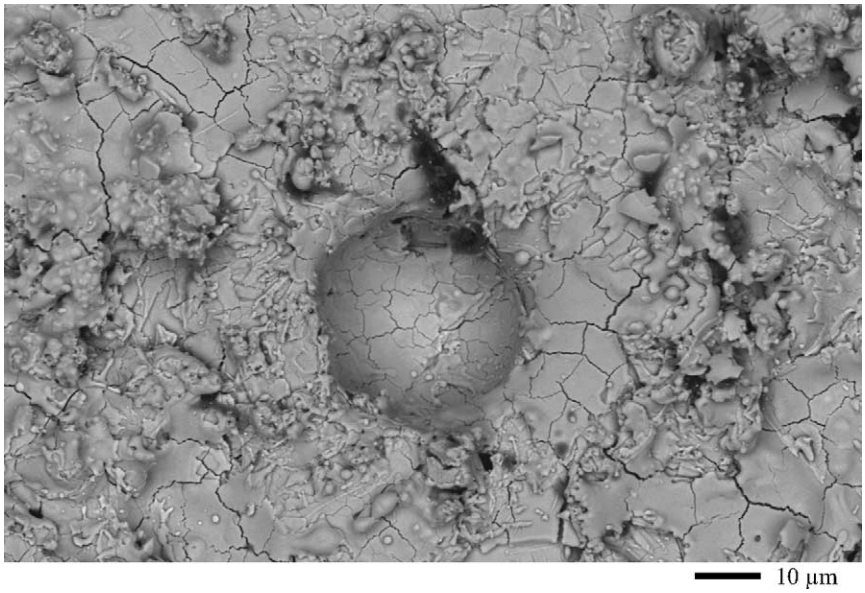

Fig. 3. Crater formation during in situ laser treatment.

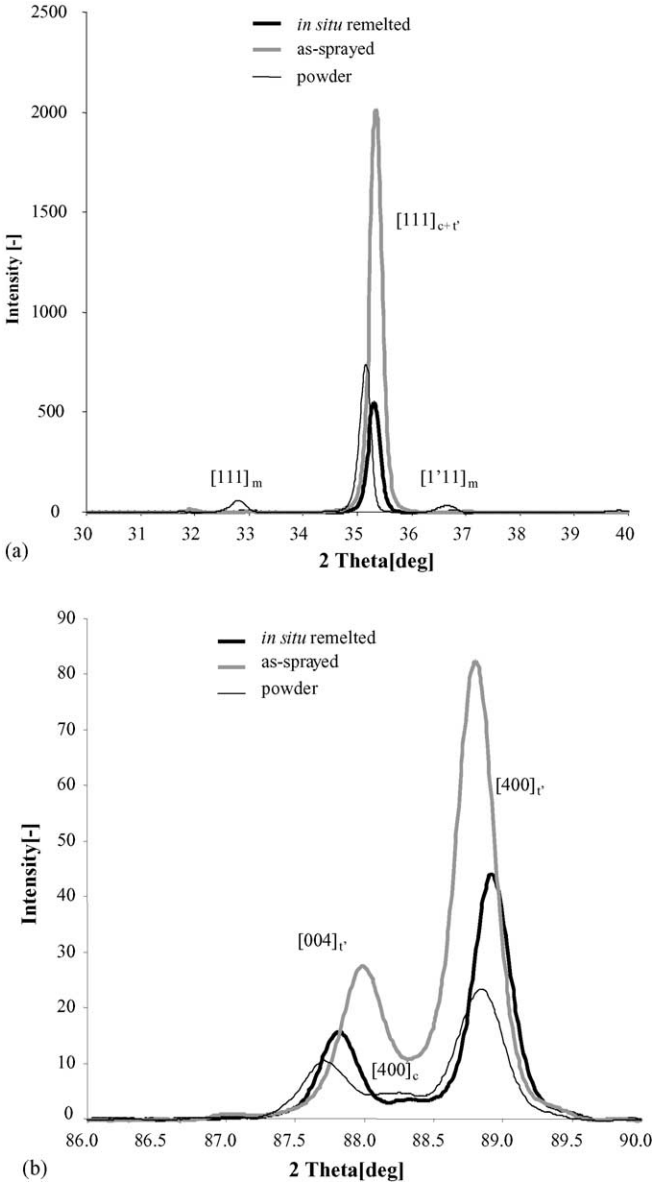

Fig. 4. Diffractogrammes for powder, as-sprayed and in situ remelted coatings: (a) 30–40° and (b) 86–90°.

3.4.2. *in situ laser remelted coatings*

In situ laser remelted coatings are mainly composed of the metastable tetragonal phase (Fig. 4). Nevertheless, a little amount of cubic phase (i.e., 10 mol%) appears, whereas no monoclinic phase is detected (i.e., the amount is lower than 1–2 mol% if monoclinic phase exists). This result seems to indicate a little come back of the t′ phase toward the equilibrium. But this observation has to be moderated by the fact that, for these diffraction angles, there is an accumulation of the diffraction lines: the phase identification becomes more difficult. Besides, a shift in the position of the $[0\ 0\ 4]_{t'}$ and $[4\ 0\ 0]_{t'}$ peaks for in situ remelted coatings is noticed compared to as-sprayed coatings. These minor shifts correspond to small variations of the t′ phase tetragonality: it is certainly linked to little variations of the yttria content because of some disparities in the solidification kinetics [6].

Table 2
Phase composition resulting from several laser treatments

	Laser energy density (J mm^{-2})	m (mol%)	c (mol%)	t′ (mol%)
Powder	n.a.	12	3	85
As-sprayed	n.a.[a]	0	0	100
In situ remelted	2.5	0	10	90

n.a.: non-applicable.
[a] Spray velocity and scanning velocity equivalent to the ones resulting from a laser energy density of 2.2–2.5 J mm^{-2}.

3.4.3. *Check of the presence of the t′ phase thanks to the evaluation of the yttria content*

The results of the evaluation of the yttria content are listed in Table 3. In all cases, the yttria content is higher than 7 wt.%. It is even equal to about 10 wt.% for as-sprayed coatings. Since the solubility limit of yttria in the tetragonal phase at equilibrium is 4 wt.%, the calculated yttria contents correspond to the presence of metastable tetragonal phase.

3.4.4. *Syntheses*

To summarize, the evolution of the studied diffraction peaks presents the following specificities:

(i) peak broadening is observed in most of the studied diffractogrammes for as-sprayed and in situ laser remelted coatings. This broadening can be explained either by the existence of micro-stresses into the coating, by the accumulation of neighboured diffraction lines, by a variation of the grain size, by a combination of these three phenomena. However, due to the

Table 3
Evaluation of the yttria content for as-sprayed and in situ laser remelted coatings

	Laser energy density (J mm^{-2})	a_t (A)	c_t (A)	c_t/a_t	Y_2O_3	
					(% mol)	(wt.%)
Powder	n.a.	5.11160	5.16412	1.01027	4.8	7.2
As-sprayed	n.a.[a]	5.11384	5.15104	1.00727	5.9	10.7
In situ remelted	2.1	5.10796	5.15752	1.00970	5.0	7.8
	2.5	5.11452	5.16352	1.00958	5.0	7.9

n.a.: non-applicable.
[a] Spray velocity and scanning velocity equivalent to the ones resulting from a laser energy density of 2.2–2.5 J mm^{-2}.

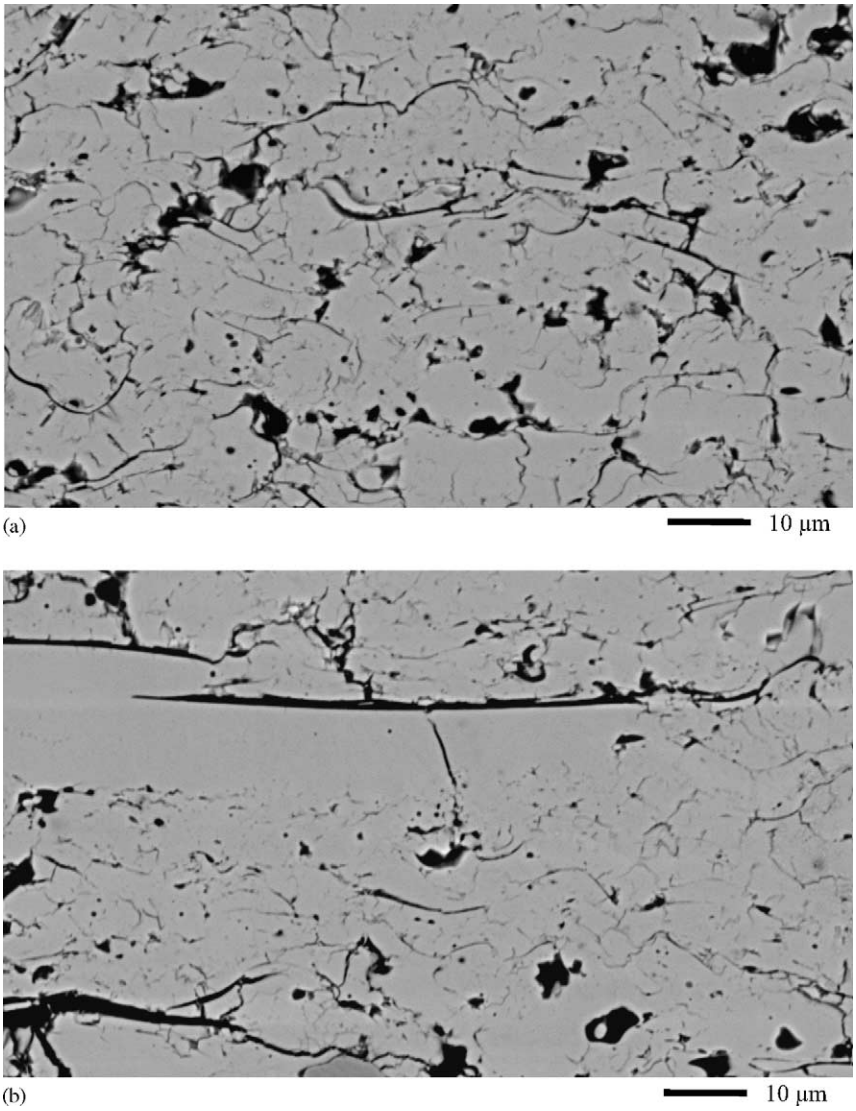

Fig. 5. Typical cross-section morphologies of (a) as-sprayed and (b) in situ remelted TBCs.

accumulation of the diffraction lines corresponding to the metastable tetragonal (i.e., with several yttria contents), the equilibrium tetragonal and the cubic phases seems to be the main phenomenon of this broadening;

(ii) the separation of the tetragonal doublet is the result of the tetragonality variation. This variation, which reveals an yttria content fluctuation in the fluorine mesh, is due to different thermal histories during the implemented process, and so to more or less long time for yttria to diffuse.

As concerns the width of the tetragonal doublet, the fact that the (0 0 4) peak shifts more than the (4 0 0) peak could be due to the higher parametric variation along the *c*-axis during the expansion. As a matter of fact, the cohesive strength is lower along the *c*-axis because of its longer length. This induces a wider shift of the first diffraction line.

3.5. Pore-crack network architecture

Fig. 5 shows typical pore network architectures of Y-PSZ as-sprayed and in situ laser remelted coatings constituted by two types of pore morphologies: (i) the globular morphology, which corresponds to pores of about ten micrometers diameter, average value; (ii) the microcracks.

Fig. 6 displays the evolution of the coating porosity level as a function of the laser energy density. It clearly appears that the in situ remelting process induces a significant modification of the TBC pore architecture. As a matter of fact, whereas the porosity level related to microcracks is stable, around 4–5%, it clearly appears that the total porosity increases from about 8% for the as-sprayed coatings to about 15% for the remelted coatings. Besides, the total porosity raises from 15% to more than 20% for a laser energy higher than 2.20 J mm^{-2}. This is directly related to an enhancement of the globular porosity level. As a matter of fact, when the

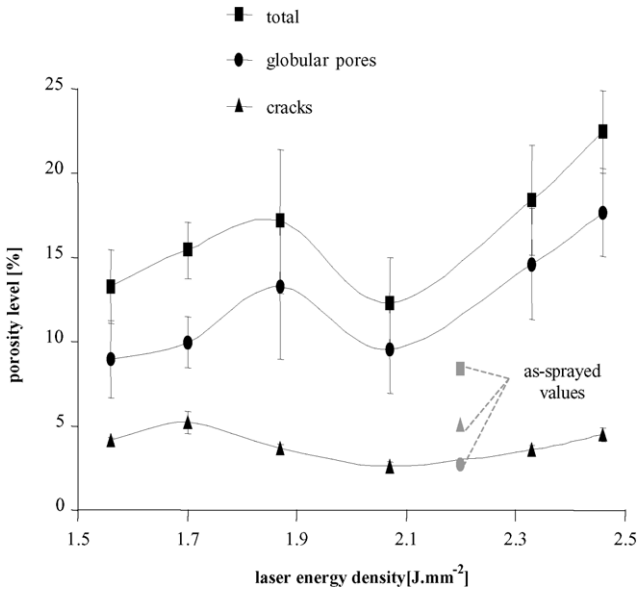

Fig. 6. Evolution of the porosity level as a function of the laser energy density input.

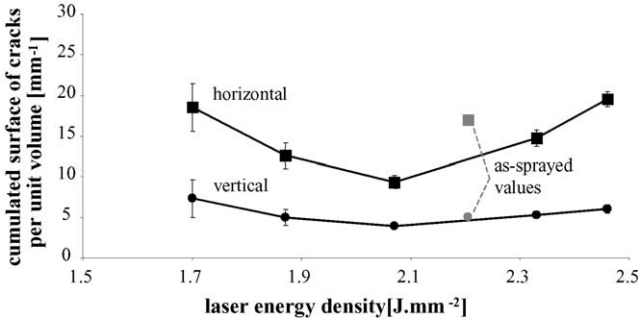

Fig. 7. Evolution of the cumulated surface of cracks per unit volume as function of the laser energy density input.

laser energy reaches high levels, thermal shocks and remelted thicknesses increase, inducing the formation of large cracks into the deposits. Those cracks are large enough to be assimilated to globular pores.

Concerning the crack network orientation, horizontal and vertical cracks were discerned. Whatever the laser energy density is, the proportion is always the same: one-third of vertical cracks and two thirds of horizontal cracks. However, remelted coatings exhibit a parabolic evolution of the cumulated surface of cracks as a function of the laser energy density (Fig. 7). A minimum appears for a laser energy density of 2.07 J mm^{-2}: i.e., a cumulated surface of cracks of 12 mm^{-1} for the horizontal cracks and of 5 mm^{-1} for the vertical cracks. This minimum seems to correspond to a compromise between two phenomena: the densification into the remelted areas and the cracks formation due to thermal shocks during laser remelting.

4. Conclusions

Y-PSZ TBCs were manufactured implementing a hybrid plasma spray process, which combines thermal spraying and laser remelting. The induced structural modifications have been investigated.

This hybrid process permits to modify:

(i) the lamellar structure of the as-sprayed coating to a columnar dendritic structure. A subdivision of the columns is observed near the surface of the remelted layer. This phenomenon can be explained by the decrease of the solid/liquid interfacial energy near the surface;
(ii) the pore-crack network architecture of thermal spray coatings. The overall porosity level increases for the in situ remelting process. Whereas a densification is observed into the laser remelted areas, large cracks are formed between them for a laser energy density higher than 2.2 J mm^{-2}. This is mostly due to thermal shocks during laser remelting.

Moreover, XRD analyses reveal that the main phase remains the metastable tetragonal (t′) phase for as-sprayed and in situ laser remelted coatings (this t′ phase is searched out for its tenacity). Only little shifts of the tetragonal doublet is noticed: they correspond to small tetragonality variations, which are certainly linked to some little variation of the yttria content because of the several solidification kinetics resulting from the implemented process (i.e., with or without in situ remelting).

Acknowledgements

Authors gratefully thank IREPA Laser (Frédérique MACHI), Parc Technologique, 67000 Strasbourg, France, for their very valuable collaboration in the sample manufacturing.

LERMPS is a member of the *Institut des Traitements de Surface de Franche-Comté* (ITSFC, surface treatment institute of Franche-Comté), France.

References

[1] D. Stöver, C. Funke, Directions of the development of thermal barrier coatings in energy applications, J. Mater. Process. Technol. 92/93 (1999) 195–202.
[2] U. Schulz, C. Leyens, K. Fritscher, M. Peters, B. Saruhan-Brings, O. Lavigne, J.-M. Dorvaux, M. Poulain, R. Mévrel, M. Caliez, Some recent trends in research and technology of advanced thermal barrier coatings, Aerospace Sci. Technol. 7 (1) (2003) 73–80.
[3] V. Teixeira, M. Andritschky, H. Gruhn, W. Mallener, H.P. Buchkremer, D. Stöver, Failure of physical vapor deposition/plasma-sprayed thermal barrier coatings during thermal cycling, J. Therm. Spray Technol. 9 (2) (2000) 191–197.

[4] A.G. Evans, D.R. Mumm, J.W. Hutchinson, G.H. Meier, F.S. Pettit, Mechanisms controlling the durability of thermal barrier coatings, Progr. Mater. Sci. 46 (2001) 505–553.
[5] G. Antou, G. Montavon, F. Hlawka, A. Cornet, C. Coddet, O. Fréneaux, Processing of Y-PSZ thermal barrier coatings implementing a high power laser diode: process parameters, in: B.R. Marple, C. Moreau (Eds.), in: Proceedings of Thermal Spray 2003: Advancing the Science and Applying the Technology, Pub. ASM International, Materials Park, OH, USA, 2003, 2003, pp. 1609–1616.
[6] H. Ibegazene, Etude microstructurales de la stabilité thermique de phases métastables dans des systèmes à base de ZrO_2, HfO_2 et d'oxydes de terres rares: application aux barrières thermiques (Microstructural investigation of thermal stability in ZrO_2, HfO_2 and rare earth sesquioxides based metastable phases: in relation to thermal barrier coatings), Ph.D. Thesis, Université Paris-Sud (U.F.R. d'Orsay), France, 1999 (in French).
[7] S.O. Chwa, A. Ohmori, The influence of surface roughness of sprayed zirconia coatings on laser treatment, Surf. Coat. Technol. 148 (2001) 88–95.
[8] H. Toraya, M. Yoshimura, S. Somiya, Quantitative analysis of monoclinic-stabilized cubic ZrO_2 systems by X-ray diffraction, J. Am. Ceram. Soc. 67 (6) (1984) 183–184.
[9] R.A. Miller, J.L. Smialek, R.G. Garlick, Phase stability in plasma sprayed partially stabilized zirconia—yttria, Science and Technology of Zirconia, Adv. Ceram. 3 (1981) 241–253.
[10] G. Teufer, The crystal structure of tetragonal ZrO_2, Acta Crystallogr. 15 (1997) 1187.
[11] H.G. Scott, Phase relationships in the zirconia–yttria system, J. Mater. Sci. 10 (1975) 1527–1535.
[12] E.E. Underwood, Stereology or the quantitative evaluation of microstructures, J. Microsc. 89 (2) (1969) 161–180.
[13] M. Gaümann, P. Gilgien, W. Kurz, La Solidification des métaux traités par laser (On the solidification of metals treated by laser), CLP Bulletin de Liaison 34 (2000) 9–24 (in French).
[14] C. Robert, A. Denoirjean, A. Vardelle, G.X. Wang, S. Sampath, Nucleation and phase selection in plasma-sprayed alumina: modeling and experiment, in: C. Coddet (Ed.), Thermal Spray: Meeting the Challenges of the 21st Century, Pub. ASM International, Materials Park, OH, USA, 1998, pp. 407–412.
[15] K.C. Chang, W.J. Wei, C. Chen, Oxidation behavior of thermal barrier coatings modified by laser remelting, Surf. Coat. Technol. 102 (1998) 197–204.
[16] K.A. Khor, S. Jana, Pulsed laser processing of plasma sprayed thermal barrier coatings, J. Mater. Process. Technol. 66 (1997) 4–8.
[17] M. Friis, C. Persson, J. Wigren, Influence of the plasma spray process on the microstructure of thermal barrier coatings, Surf. Coat. Technol. 141 (2001) 115–127.
[18] L. Lelait, Etude microstructurale fine de revêtements céramiques du type barrière thermique: incidence sur la résistance thermomécanique de ces revêtements (Microstructural study of thermal barrier coatings: application of the thermomechanical resistance of these coatings), Ph.D. Thesis, Université Paris-Sud (U.F.R. d'Orsay), France, 1991 (in French).
[19] M. Poulain, Etude de la conductivité thermique de revêtements céramiques à base de zircone: relation avec la composition, la microstructure et la morphologie (Thermal conductivity of zirconia based coatings in relation with composition, structure and morphology), Ph.D. Thesis, Université Paris-Sud (U.F.R. d'Orsay), France, 1999 (in French).